Electron energy band alignment at the (100)Si/MgO interface

V. V. Afanas'ev' , A. Stesmans, K. Cherkaoui, and P. K. Hurley

Citation: Appl. Phys. Lett. **96**, 052103 (2010); doi: 10.1063/1.3294328
View online: http://dx.doi.org/10.1063/1.3294328
View Table of Contents: http://aip.scitation.org/toc/apl/96/5
Published by the American Institute of Physics

Electron energy band alignment at the (100)Si/MgO interface

V. V. Afanas'ev,[1,a)] A. Stesmans,[1] K. Cherkaoui,[2] and P. K. Hurley[2]
[1]*Department of Physics, University of Leuven, Celestijnenlaan 200D, B-3001 Leuven, Belgium*
[2]*Tyndall National Institute, University College Cork, Lee Maltings, Prospect Row, Cork, Ireland*

(Received 5 November 2009; accepted 27 December 2009; published online 1 February 2010)

The electron energy band diagram at the (100)Si/MgO interface is characterized using internal photoemission of electrons and holes from Si into the oxide. For the as-deposited amorphous MgO the interface barriers correspond to a band gap width of 6.1 eV, i.e., much lower than the conventionally assumed bulk crystal value (7.83 eV). The annealing-induced crystallization of MgO mostly affects the energy of the valence band while the conduction band bottom retains its energy position at 3.37 ± 0.05 eV above the top of the silicon valence band. © *2010 American Institute of Physics*. [doi:10.1063/1.3294328]

Thanks to the ease of epitaxial growth on various crystal substrates[1] and the wide bulk crystal band gap (7.83 eV)[2] magnesium oxide, MgO, has attracted considerable interest as a material for a broad spectrum of electronic applications ranging from gate insulators in metal-oxide-semiconductor (MOS) transistors[3–5] to a buffer layer enabling integration of other functional oxides.[6,7] In particular, MgO is widely used as a barrier in magnetic tunnel junctions (MTJs)[8–10] with the recently demonstrated possibility of spin injection into the silicon crystal.[11,12] In all these applications, MgO is supposed to serve as an insulator providing high energy barriers for electrons and holes. Though the knowledge of the barriers is of particular importance for MTJs as they determine the type of charge carriers that provide the dominant contribution to the tunneling current,[11] the band alignment between MgO and silicon, the most relevant for device fabrication, has not been addressed yet experimentally. One of the reasons for this lack of information concerns the strong impact of the x-ray induced insulator charging[13] which in the case of MgO has been quoted as "commonly catastrophic."[14]

To avoid the charging-related errors, here we have addressed the problem using the internal photoemission (IPE) spectroscopy.[15–17] In IPE, the interface barrier height is obtained as the spectral threshold of photocurrent generated in a MOS capacitor by charge carriers photoexcited to energies above the barrier and subsequently injected into the insulating layer.[15] Depending on the orientation of electric field at the interface, one may observe IPE of electrons or holes and determine the corresponding barrier heights.[16,17] By combining the two barrier values, we have found that amorphous (a-) MgO on (100)Si has a much reduced band gap, $E_g = 6.1$ eV, compared to the above mentioned bulk crystal value. Comparison between the as-deposited a-MgO layer and that crystallized by additional postdeposition anneal (PDA) indicates that the conduction band (CB) offset remains considerably lower (2.25 eV) than the valence band (VB) offset (2.7 eV in a-MgO and higher in the crystallized layer).

Studied samples were prepared on the H-terminated (100) surface of low-doped n- or p-type Si (n_d, $n_a \sim 10^{15}$ cm^{-3}) by e-beam deposition of MgO from 99.99% purity pellets with the Si temperature kept low (~150 °C) to obtain amorphous MgO layers.[18] Some samples were subsequently crystallized by 30 min PDA in N_2 at 500 °C resulting in a columnar (granular) film of rocksalt structure.[5,18] For the IPE experiments we used relatively thick (39–40 nm) MgO layers to prevent the Si/MgO interface from hydroxylation[16] during *ex situ* metal evaporation. MOS capacitors were fabricated by thermoresistive evaporation from a W boat of semitransparent (15 nm thick) Au or Al electrodes of 0.5 mm^2 area. These were used to measure IPE spectra at room temperature in the photon energy range $h\nu = 2-6.8$ eV with a constant spectral resolution of 2 nm. The quantum yield (Y) is defined as the photocurrent normalized to the incident photon flux and analyzed as a function of $h\nu$ and the strength of the electric field (F) in the MgO.

Logarithmic plots of the yield are shown in Fig. 1 for MOS capacitors with as-deposited amorphous (a) and crystallized (b) MgO insulators, as measured under the indicated

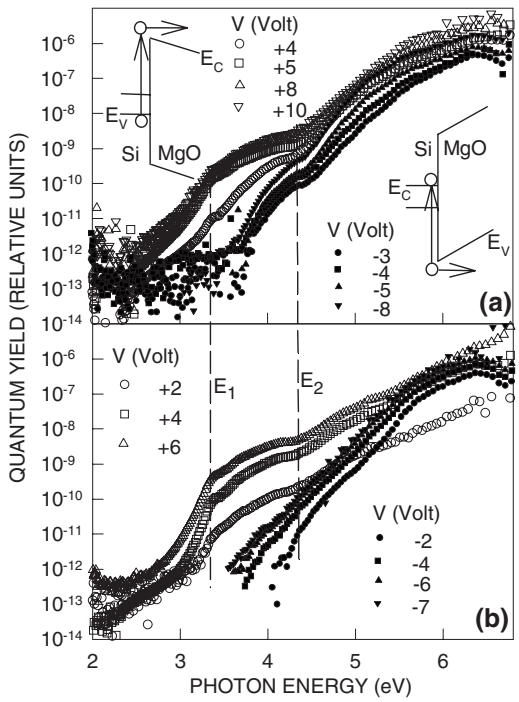

FIG. 1. Logarithmic plot of the IPE quantum yield as a function of photon energy measured in as-deposited (a) (100)Si/MgO/Au samples and (b) after crystallization of the oxide insulators by PDA at 500 °C as measured under the indicated positive (open symbols) and negative (filled symbols) bias applied to the top Au electrode. Vertical lines mark the onsets of E_1 and E_2 direct optical transitions Λ_3-Λ_1 and Σ_2-Σ_3, respectively, in the Si substrate crystal. Insets in panel (a) show schematics of the electron transitions.

a)Electronic mail: valeri.afanasiev@fys.kuleuven.be.

positive (open symbols) or negative (filled symbols) bias applied to the top Au electrode. In the photon energy range $h\nu < 4.5$ eV the curves measured under opposite orientation of electric field diverge suggesting that the photocurrent is dominated by IPE from the electrodes of the MOS capacitor. As replacement of the top electrode material from Au to Al has no effect on the curves measured under positive metal bias (not shown), electron states of the metal are unlikely to contribute to the IPE current thus indicating the electron IPE at the Si/MgO interface to be the major signal source. This conclusion is consistent with the observed modulation of the spectra at photon energies of $E_1 = 3.4$ eV and $E_2 = 4.3$ eV (cf. vertical lines in Fig. 1) due to the excitation of the direct optical transitions Λ_3-Λ_1 and Σ_2-Σ_3, respectively, in the Si crystal.[16,17] These transitions cause a significant increase in reflectivity and optical absorption of Si but do not provide electrons of energy sufficient to overcome the interface barrier and, therefore, result in a decrease in the yield with increasing photon energy. The spectral threshold of electron IPE corresponds to the energy barrier between the top of the Si VB and the bottom of the MgO CB [cf. inset in the upper left corner in Fig. 1(a)] and can be found from the $Y^{1/3}$-$h\nu$ plots[15,19] shown by the open symbols in Fig. 2 for the as-deposited (a) and crystallized (b) MgO. Though the electron IPE threshold is better exposed in the spectra of the crystallized layer [cf. Fig. 2(b)] than in those of a-MgO [panel (a)], the values obtained by linear extrapolation to the subthreshold level appear to be the same within experimental accuracy.

The IPE spectra measured under negative metal bias (filled symbols in Figs. 1 and 2) indicate [cf. panels (a)] that in the as-deposited sample the yield exhibits an enhancement at $E_2 \approx 4.3$ eV suggestive of *hole* IPE from Si.[17] However, upon crystallization this feature disappears although a somewhat reduced photocurrent remains measurable in the range $3.5 < h\nu < 4.5$ eV. This behavior can be explained by photocurrent arising in the same spectral range not only from hole IPE from the CB of Si into the MgO VB [cf. insert in the bottom right corner in Fig. 1(a)] but, also from electron IPE from Au to the MgO CB since the Au/MgO interface is characterized by a barrier height of 4.0 eV.[20] To separate electron and hole IPE signals it appears instructive to compare the yield spectra measured under the same bias of −7 V in samples with Au and Al electrodes prior and after MgO crystallization. The logarithmic plots of these spectra, shown in Fig. 3, reveal that crystallization of the MgO layer has no noticeable effect on the barrier height between the Fermi level of Al and the bottom of the MgO CB; the barrier is found to be 2.7 ± 0.1 eV (the Fowler plots are not shown) in good agreement with the literature.[20] By contrast, in the case of the Au electrode one may notice the disappearance upon annealing of the portion of current characterized by the well expressed E_2 singularity related feature. Therefore, we conclude that the crystallization of MgO suppresses the hole IPE from Si due to a shift of the MgO VB top. Since the hole IPE in the as-deposited samples provides the dominant photocurrent in the spectral range $4 < h\nu < 5$ eV, for this case one still can evaluate the IPE spectral threshold from the $Y^{1/2}$-$h\nu$ plots[19] as shown by the filled symbols in Fig. 2(a).

The field dependence of the electron IPE thresholds is shown in Fig. 4 in the form of Schottky plots for the amorphous (○) and crystallized (□) MgO. The measured electron IPE thresholds are seen to obey the classical image-force

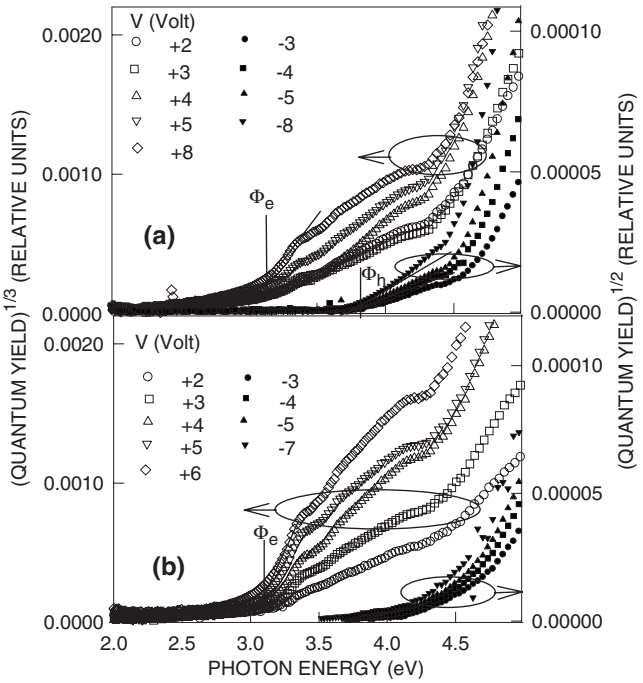

FIG. 2. Cube (left scale) and square root (right scale) plots of the IPE quantum yield as a function of photon energy measured in (100)Si/MgO/Au samples in the as-deposited state (a) and after MgO crystallization by PDA at 500 °C (b) under the indicated voltages applied to the Au electrode. Vertical lines mark the onsets of E_1 and E_2 direct optical transitions within the Si crystal and the spectral thresholds of electron (Φ_e) and hole (Φ_h) IPE.

barrier model,[15,21] yielding a zero-field barrier height of $\Phi_e = 3.37 \pm 0.05$ eV and the high-frequency dielectric constant $\varepsilon_{MgO} = 4.0 \pm 0.2$. As one expects $\varepsilon_i \approx n^2$,[15] the latter is in fair agreement with the measured refractive index $n_{MgO} = 1.8$ at $h\nu = 5.0$ eV. From the inferred energy barrier between the Si VB top and the MgO CB bottom the CB offset at the (100)Si/MgO interface can be calculated as $\Delta E_C = \Phi_e - E_g(Si) = 2.25 \pm 0.05$ eV.

The top of the image force barrier is located at a distance of $x_m = (q/16\pi\varepsilon_0\varepsilon_{MgO}F)^{1/2}$ from the surface of emitter, where q is the elemental charge and ε_0 is the vacuum permittivity.[15,17,21] As a result, the barrier height measured by IPE corresponds to the energy position of the MgO CB at the distance x_m from the silicon surface. In our experiments the strength of the electric field F in MgO increases from 0.1 to 2.5 MV/cm, which corresponds to a decrease in x_m from 3 to

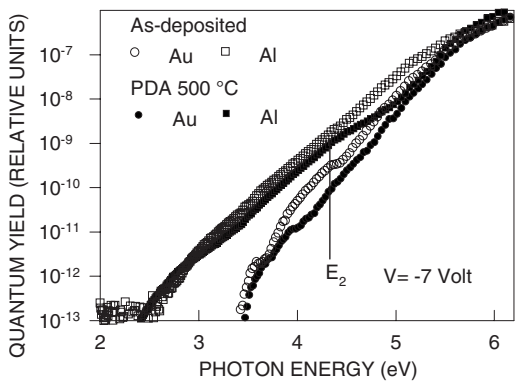

FIG. 3. Logarithmic plot of the IPE quantum yield as a function of photon energy measured in (100)Si/MgO/Au samples with as-deposited (open symbols) and crystallized (filled symbols) MgO under −7 V bias applied to the Au (circles) or Al (squares) electrode. The vertical line marks the onset of the E_2 direct optical transition in the Si substrate crystal.

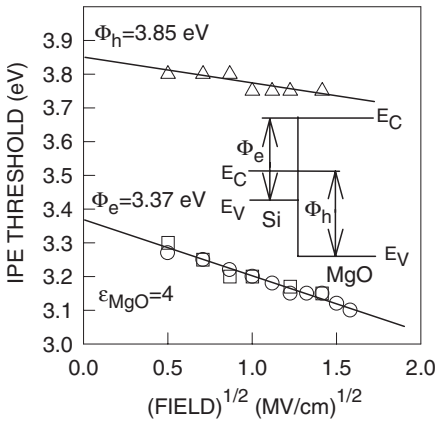

FIG. 4. Schottky plot of the electron (○,□) and hole (△) IPE thresholds measured in (100)Si/MgO/Au samples with as-deposited (○,△) and crystallized (□) MgO layers. The insert shows a schematic of the Si/MgO interface band diagram with the electron (Φ_e) and hole (Φ_h) IPE barriers indicated by arrows.

0.6 nm. Following the argumentation of DiStefano,[21] as no measurable deviation from the ideal image-force behavior is observed, one may conclude that the MgO CB edge remains at the same energy at distances larger than 0.6 nm from the Si/MgO interface plane. The depth of the thus probed MgO layer from 0.6 to 3 nm covers the range of the of the tunnel oxide thickness typically used in MTJs[9–11] making the IPE analysis relevant not only to the gate insulator stacks but, also, to the thin oxide structures.

The inferred spectral threshold of the hole IPE exhibits a weaker field dependence compared to the electron IPE case (cf. △ in Fig. 4). This effect is consistent with the expected slow motion of a hole in the oxide VB, possibly as a polaron, thus allowing polarization of the silicon.[17] The barrier between the Si CB bottom and the MgO VB top obtained by extrapolation to zero field is equal to $\Phi_h = 3.85 \pm 0.10$ eV. Combined with the inferred electron IPE barrier the latter value allows us to obtain the band gap of a-MgO as $E_g(\mathrm{MgO}) = \Phi_e + \Phi_h - E_g(\mathrm{Si}) = 6.1 \pm 0.1$ eV, i.e., significantly smaller than the commonly quoted crystal gap of 7.83 eV.[2]

For $h\nu > 5$ eV, the photocurrents under positive and negative metal bias become close. They appear to exhibit the same spectral distribution (cf. Fig. 1), suggesting that the signal arises from the generation of mobile charge carriers in the MgO layer. From the $Y^{1/2}$-$h\nu$ plots (not shown) the spectral thresholds of these currents are found to be about 4.5 and 5.3 eV for the as-deposited and the crystallized samples, respectively. Yet, in the absence of additional structural or chemical information we refrain from speculations regarding the atomic origin of electron states responsible for this MgO photoconductivity.

The band gap narrowing in the as-deposited a-MgO compared to the bulk crystal represents the most intriguing result of this work. We have noted earlier that the band gap in amorphous light-metal oxides is significantly lower than in the bulk crystal. In Al_2O_3 the gap decreases from 8.8 eV in sapphire to 6.0–6.2 eV in deposited amorphous alumina[22] (values as low as 5.6 eV can be found in the literature[23]). In a-Sc_2O_3 on Si the gap is 5.6–5.7 eV, observed to widen to 6.0–6.1 eV in the film crystallized by supplemental PDA. Most of the gap variation is associated, again, with a shift of the VB top.[24] The MgO layers are seen to follow the same trend: Upon crystallization the gap increases from 6.1 eV to a value likely close to the one of the bulk crystal (7.83 eV) with the result that hole IPE becomes undetectable.

The inferred hole IPE barrier Φ_h at the (100)Si/a-MgO interface allows us to calculate the VB offset as 2.7 eV, which is likely to increase upon crystallization. With a CB offset of 2.2 eV the interface band diagram emerges as asymmetric, with a lower barrier for electrons than for holes. However, if a metal with large work function is used as emitter in the MTJ structure, the band gap narrowing in noncrystallized MgO may result in a lower barrier for holes than for electrons. For instance, the inferred value $E_g(\mathrm{MgO}) = 6.1$ eV would make the latter case relevant to the Au/MgO and Fe/MgO interfaces characterized by electron barriers exceeding $E_g(\mathrm{MgO})/2$.[20]

The work at KU Leuven was supported by the "Fonds Wetenschappelijk Onderzoek (FWO)-Vlaanderen" through Grant No. 1.5.057.07. The authors from the Tyndall National Institute acknowledge the support of Science Foundation Ireland (SFI) under the FORME Strategic Research Cluster Award No. 07/SRC/I1172.

[1] See, e. g., D. P. Norton, Mater. Sci. Eng. R. **43**, 139 (2004), and references therein.
[2] R. C. Whited, C. J. Flaten, and W. C. Walket, Solid State Commun. **13**, 1903 (1973).
[3] L. Yan, C. M. Lopez, R. P. Shrestha, E. A. Irene, A. A. Suvorova, and M. Saunders, Appl. Phys. Lett. **88**, 142901 (2006).
[4] A. Posadas, F. J. Walker, C. H. Ahn, T. L. Goodrich, Z. Cai, and K. S. Ziemer, Appl. Phys. Lett. **92**, 233511 (2008).
[5] E. Miranda, E. O'Connor, K. Cherkaoui, S. Monaghan, R. Long, D. O'Connell, P. K. Hurley, G. Hughes, and P. Casey, Appl. Phys. Lett. **95**, 012901 (2009).
[6] T. L. Goodrich, Z. Cai, and K. S. Ziemer, Appl. Surf. Sci. **254**, 3191 (2008).
[7] T. C. Zhang, Y. Guo, Z. X. Mei, C. Z. Gu, and X. L. Du, Appl. Phys. Lett. **94**, 113508 (2009).
[8] X. Jiang, R. Wang, R. M. Shelby, R. M. Macfarlane, S. R. Bank, J. S. Harris, and S. S. P. Parkin, Phys. Rev. Lett. **94**, 056601 (2005).
[9] R. Wang, X. Jiang, R. M. Shelby, R. M. Macfarlane, S. S. P. Parkin, S. R. Bank, and J. S. Harris, Appl. Phys. Lett. **86**, 052901 (2005).
[10] P. Padhan, P. LeClair, A. Gupta, K. Tsunekawa, and D. D. Djayaprawira, Appl. Phys. Lett. **90**, 142105 (2007).
[11] T. Uhrmann, T. Dimopoulos, H. Btuckl, V. K. Lazarov, A. Kohn, U. Paschen, S. Weyers, L. Bar, and M. Ruhrig, J. Appl. Phys. **103**, 063709 (2008).
[12] T. Sasaki, T. Oikawa, T. Suzuki, M. Shirashi, Y. Suzuki, and K. Tagami, Appl. Phys. Express **2**, 053003 (2009).
[13] W. M. Lau, J. Appl. Phys. **65**, 2047 (1989).
[14] L. H. Tjeng, A. R. Vos, and G. A. Sawatzky, Surf. Sci. **235**, 269 (1990).
[15] R. J. Powell, J. Appl. Phys. **41**, 2424 (1970).
[16] V. V. Afanas'ev and A. Stesmans, J. Appl. Phys. **102**, 081301 (2007).
[17] V. V. Afanas'ev, *Internal Photoemission Spectroscopy: Principles and Applications* (Elsevier, Amsterdam, 2008).
[18] P. Casey, E. O'Connor, R. Long, B. Brennan, S. A. Krasnikov, D. O'Connell, P. K. Hurley, and G. Hughes, Microelectron. Eng. **86**, 1711 (2009).
[19] J. S. Helman and F. Sanchez-Sinencio, Phys. Rev. B **7**, 3702 (1973).
[20] Y. Lu, J. C. Le Breton, P. Turban, B. Lepine, P. Schieffer, and G. Jezequel, Appl. Phys. Lett. **89**, 152106 (2006).
[21] T. H. DiStefano, J. Vac. Sci. Technol. **13**, 856 (1976).
[22] V. V. Afanas'ev, M. Houssa, A. Stesmans, and M. M. Heyns, J. Appl. Phys. **91**, 3079 (2002).
[23] M. Aguilar-Frutis, M. Garsia, and C. Falcony, Appl. Phys. Lett. **72**, 1700 (1998).
[24] V. V. Afanas'ev, S. Shamuilia, M. Badylevich, A. Stesmans, L. F. Edge, W. Tian, D. G. Schlom, J. M. J. Lopes, M. Roeckerath, and J. Schubert, Microelectron. Eng. **84**, 2278 (2007).